

treatment of cancer [9], emit a very weak fluorescence (a quantum yield of 2.1×10^{-3}) in the wavelength region from 600 to 700 nm. A continuous train of excitation pulses at 570 nm, to avoid photodegradation due to irradiation around 400 nm, is focussed by a lens into the sample cell containing the circulating HpD dye solution. The line of focus is directed just inside the output face of the cell to minimize any reabsorption of the fluorescence. The fluorescence band from the porphyrins is efficiently selected by using an interference filter which eliminates the excitation radiation at 570 nm. The fluorescence at 90° with respect to the input direction is focussed on the input slit (slit width $\sim 20 \mu\text{m}$) of the streak camera by a lens after passing through a polarizer set at 55° and the filter. When the gain of the MCP has been set at maximum, the decaying fluorescence profiles have been observed on the TV monitor, as shown in Fig. 3. From the decay, a fluorescence lifetime of HpD in PBS has been determined to be 239 ps. It is found from the comparison with a fluorescence lifetime obtained by calculations for a similar metal-free porphyrin [10] that the measured value appears to be reasonable.

CONCLUSION

A compact synchroscan streak camera has been developed, and it has been shown by measuring durations of pulses from

the HML CW dye laser that its overall time resolution is 10.8 and 25.9 ps for ~ 160 and $\sim 10^8$ superimpositions, respectively. In addition, it has been demonstrated that the camera system is useful for observing a very fast and weak fluorescence profile of a biomolecule.

REFERENCES

- [1] S. L. Shapiro, Ed., "Ultrashort light pulses," in *Topics in Applied Physics*, vol. 18. Berlin: Springer, 1977.
- [2] M. C. Adams, W. Sibbett, and D. J. Bradley, *Opt. Commun.*, vol. 26, p. 273, 1978.
- [3] J. R. Taylor, M. C. Adams, and W. Sibbett, *Appl. Phys. Lett.*, vol. 35, 590, 1979.
- [4] W. Sibbett, J. R. Taylor, and D. Welford, *IEEE J. Quantum Electron.*, vol. QE-17, p. 500, 1981.
- [5] Y. Tsuchiya *et al.*, presented at 15th Int. Congr. on High Speed Photography and Photonics, Aug. 1982, San Diego, CA. K. Kinoshita *et al.*, presented at 15th Int. Congr. on High Speed Photography and Photonics, Aug. 1982, San Diego, CA.
- [6] M. Yamashita and T. Sato, *Appl. Opt.*, vol. 21, p. 2092, 1982.
- [7] E. Inuzuka *et al.*, "Direct readout system for streak cameras," *SPIE*, vol. 189, p. 586, 1978.
- [8] M. Gouterman, in *The Porphyrins* (vol. III of *Physical Chemistry, Part A*, D. Dolphin Ed. New York: Academic Press, 1978, pp. 24-47.
- [9] T. J. Dougherty and R. E. Thoma, in *Laser in Photomedicine and Photobiology*, R. Pratesi and C. A. Sacchi, Eds. (Springer Ser. in Optical Sciences vol. 22). Berlin: Springer, 1980, pp. 67-75.
- [10] P. G. Seijbold and M. Gouterman, *J. Mol. Spectr.*, vol. 31, p. 1, 1969.

The Measurement and Deconvolution of Time Jitter in Equivalent-Time Waveform Samplers

WILLIAM L. GANS, MEMBER, IEEE

Abstract—The presence of time jitter between the trigger signal and the sampling strobe in an equivalent-time sampling oscilloscope can cause appreciable distortion of the recorded waveform. Under additive signal averaging conditions, a method has been developed to reduce this distortion. The method consists essentially of deconvolving a jitter-related effective impulse response from the recorded waveform data.

I. INTRODUCTION

THE NBS Electromagnetic Waveform Metrology Group's Automatic Pulse Measurement System (APMS) is the primary system used for repetitive waveform measurements and calibrations in the time epoch range of 100 ps to 1 μs

[1]–[3]. It consists of a wide-band (dc–18-GHz) equivalent-time sampling oscilloscope interfaced to a minicomputer system via a 14-bit D/A and A/D converter unit. The interfacing of these three units is such that fast pulse waveforms may be acquired on the sampling oscilloscope and recorded into the minicomputer memory, usually as Fortran arrays, for subsequent processing and analysis.

As with any measurement system, it is of great interest to be able to deconvolve (or otherwise remove) the distorting effects of that system from the measurement. In 1976, Riad and Nahman developed a time-domain impulse response model for the APMS sampling oscilloscope [4], [5] and in 1979, Guillaume and Nahman devised a numerical deconvolution technique for pulse waveform data [6], [7]. Together, these two accomplishments permitted the deconvolution of the distorting effects of the wide-band sampling system from the measured recordings of fast pulse waveforms.

Manuscript received July 15, 1982; revised November 1, 1982.

The author is with the National Bureau of Standards, Electromagnetic Waveform Metrology Group, Electromagnetic Technology Division, Boulder, CO 80303.

However, there remains one large source of measured waveform distortion in the APMS; namely, that caused by the random jitter between the sampling oscilloscope trigger signal and the sampling command strobe itself. As was shown in [1] and [2], the net result of additive signal averaging in the presence of timing jitter is equivalent to adding a low-pass filter to the signal channel, smoothing and spreading out the faster portions of the waveform. The effect of timing jitter, then, may be thought of as equivalent to the series addition into the modeled APMS measurement channel of a filter network which causes the same waveform measurement distortion as the jitter. The method described in this paper consists of modeling or measuring an effective jitter-related time-domain impulse response function and then using the deconvolution algorithm of Nahman and Guillaume to remove the jitter-related distortion from the recorded waveform data.

Section II of this paper deals with the concept and theory of the jitter deconvolution technique. The results of some computer simulation studies are presented as Section III. Section IV contains some conclusions and directions for future work.

II. CONCEPT AND THEORY

A. APMS Description

The APMS, made up essentially of a minicomputer system, a 14-bit D/A-A/D unit, a wide-band sampling oscilloscope, and necessary interface circuitry, is shown in block diagram form in Fig. 1. Briefly, the system acquires and records waveform data in the following manner. Under program control, the computer sends a 14-bit digital word to the D/A converter. The analog voltage (0 to 5 V) corresponding to this digital word is sent to the sampling oscilloscope time axis circuitry where it controls the time at which the next voltage sample will occur. Zero volts will cause a sample to occur at the leftmost sampling oscilloscope CRT graticule line while 5 V (full scale) will cause a sample to occur at the rightmost graticule line. Thus the computer-D/A-sampling oscilloscope circuitry may be thought of as a digital oscilloscope sweep generator.

Once the time axis has been set by the D/A, the sampling oscilloscope trigger circuitry is enabled and the next available trigger signal is permitted to cause a voltage sample to be taken in the wide-band sampling head. This voltage sample is then converted into a 14-bit digital word by the A/D converter and stored in the computer core memory.

By sequentially stepping the D/A converter from 0 to 5 V, a complete digital waveform may be recorded up to a maximum of 16 384 equally spaced time points (2^{14} points for a 14-bit D/A converter). Similarly, the voltage axis resolution is also 1 part in 16 384 yielding a maximum system dynamic range of about 84 dBV.

The useful time windows available for waveform recording with the APMS vary from 100 ps to 1 μ s in a 1-2-5 sequence. The useful voltage input windows, with no external gain or attenuation, vary from 20 mV to 1 V, again in a 1-2-5 sequence. The maximum trigger rate, under computer control, is approximately 7 kHz. It should be noted that only repetitive waveforms may be measured with equivalent time samplers such as that employed in the APMS because only one voltage

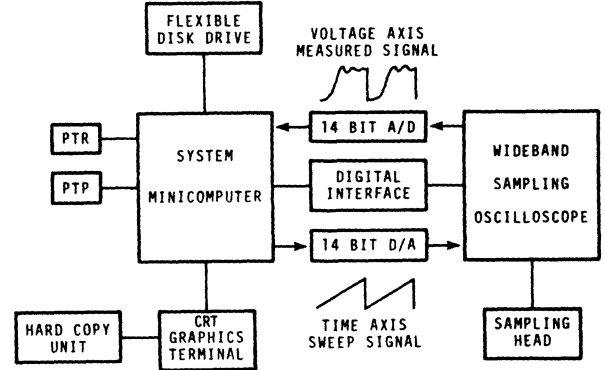


Fig. 1. Block diagram of NBS Automatic Pulse Measurement System (APMS).

sample is acquired for each occurrence of the waveform being measured.

B. Deconvolution Algorithm Description

Although the generalized subject of deconvolution is much too lengthy to be addressed in this paper, a short description of the Nahman-Guillaume algorithm is included here for completeness. For the discrete (digital) case, given a linear time-invariant system with an N -point time-domain impulse response sequence

$$h(k), \quad k = 0, 1, 2, \dots, N-1$$

and given a system input signal sequence and system output signal sequence,

$$x(k), \quad k = 0, 1, 2, \dots, N-1$$

and

$$y(k), \quad k = 0, 1, 2, \dots, N-1$$

respectively, then these three discrete functions are related by the well-known convolution summation

$$y(k) = \sum_{j=0}^k x(j) h(k-j), \quad k = 0, 1, 2, \dots, N-1. \quad (1)$$

Solving (1) for either $x(k)$ or $h(k)$ is the deconvolution problem and, for $x(k)$, may be written

$$x(k) = \frac{1}{h(0)} \left[y(k) - \sum_{j=0}^{k-1} x(j) h(k-j) \right], \quad k = 0, 1, 2, \dots, N-1 \quad (2)$$

where $h(0) \neq 0$.

In general, (2) is an ill-conditioned problem with no unique solution. Attempts to directly solve (2) for $x(k)$, say by back substitution techniques, usually lead to solutions that diverge, especially when the $y(k)$ and/or $h(k)$ data are inexact such as in the presence of noise.

The method developed by Nahman and Guillaume is essentially a frequency-domain filtering technique. By taking the discrete Fourier transforms of the two known sequences $h(k)$ and $y(k)$, the frequency-domain solution for $X(n)$ becomes

$$X(n) = \frac{Y(n)}{H(n)}, \quad n = 0, 1, 2, \dots, N-1 \quad (3)$$

and the time-domain solution, $x(k)$, is simply the inverse discrete Fourier transform of $X(n)$. Usually, however, similarly to (2), the solution of (3) is unstable and divergent.

In order to stabilize the solution of (3), Nahman and Guillaume added a frequency-domain filtering term, $R(n)$, that they refer to as a regularization operator. Thus (3) becomes

$$X(n) = \frac{Y(n)}{H(n)} R(n) \quad (4)$$

where $R(n)$ is given by

$$R(n) = \frac{|H(n)|^2}{|H(n)|^2 + \gamma|C(n)|^2} \quad (5)$$

$|C(n)|^2$ is the squared magnitude of the discrete Fourier transform of the second difference operator and may be written

$$|C(n)|^2 = 6 - 8 \cos\left(\frac{2\pi n}{N}\right) + 2 \cos\left(\frac{4\pi n}{N}\right), \quad n = 0, 1, 2, \dots, N-1. \quad (6)$$

γ is called the regularization parameter; its value is adjusted to yield the "best" answer for $x(k)$, the inverse discrete Fourier transform of $X(n)$. With $\gamma = 0$, no filtering occurs. As γ is increased, more and more filtering occurs, particularly at higher frequencies. In general, too little filtering yields a noisy, unstable result for $x(k)$ while too much filtering causes excessive distortion of the true $x(k)$ waveform. The trick is to choose a value of γ which lies between the two extremes to provide the best (subjective) solution.

In their experiments, Nahman and Guillaume discovered that for values of γ that appeared to yield the best solutions it happened that the rms value of the imaginary part of $x(k)$ passed through a minimum. Thus it is possible to provide an automatic stopping criterion in the deconvolution program. Solutions are simply iterated for increasing γ until the above-mentioned minimum is found. It is by no means clear at this time that this stopping criterion is the optimum choice and investigation of this problem is still being conducted. (The deconvolutions reported in this work were performed using this criterion.)

C. Jitter Deconvolution Technique

With the availability of the deconvolution algorithm it becomes possible to remove (mostly) the effects of time jitter from the measured, signal-averaged waveform data. Fig. 2 is a photograph of a single 1024-point sweep showing the effects of time jitter on recorded fast pulse waveforms. In this case, the waveform is from a tunnel diode pulse generator with a 10- to 90-percent transition duration of approximately 20 ps and an amplitude of about 250 mV into 50 Ω . The predominant noise in this recording is due to time jitter as may be deduced from the fact that the sample dispersion is greatest in the waveform regions where the slope is greatest; where the waveform slope is zero or nearly zero the sample dispersion is much less.

In the APMS there are really two sources of noise that must be considered. The first is voltage or y-axis noise present in the sampling oscilloscope vertical channel. The second, considered

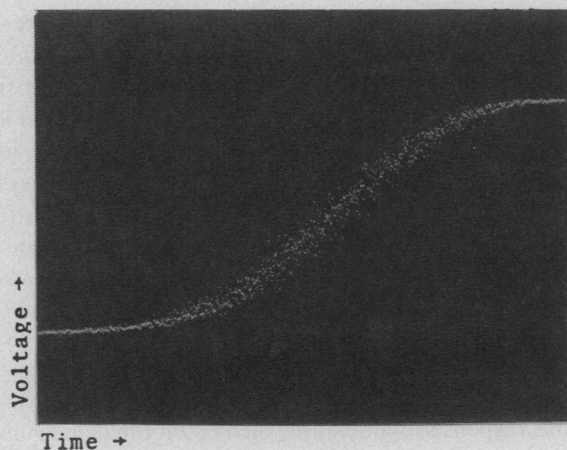


Fig. 2. 1024-point single sweep of a tunnel diode pulse generator showing the effects of time jitter. Time window is 50 ps and voltage window is 500 mV.

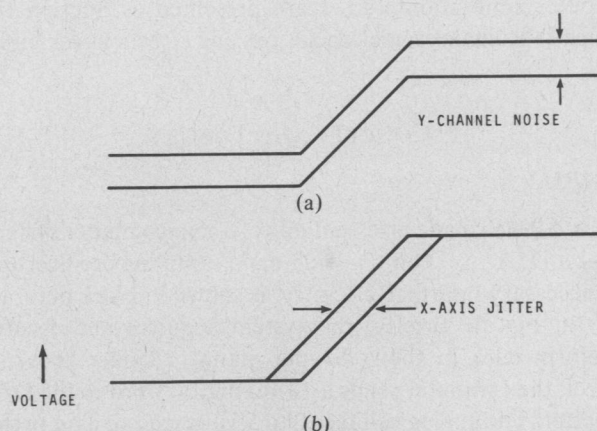


Fig. 3. Modeled ramp waveform illustrating the effects of (a) y-axis voltage noise and (b) x-axis time jitter noise.

here to be statistically orthogonal and independent of the first, is the time or x-axis jitter noise. Fig. 3(a) and (b) shows the different effects that these two noises have on a modeled recording of a ramp waveform.

Clearly, if the y-axis noise process is stationary with a zero mean about the voltage value of the measured function, then the additive averaging of a very large number of samples at each sampling time point will eventually permit convergence to the true value of the measured function, i.e.,

$$\lim_{N \rightarrow \infty} \left\{ \frac{1}{N} \sum_{j=1}^N [v_a(t) + v_j(t)] \right\} = v_a(t) \quad (7)$$

where $v_a(t)$ is the true value of the measured function at time t , v_j is the added y-axis noise component of the j th sample taken at time t , and N is the total number of samples additively averaged.

Such is not the case, however, with time jitter. For a stationary jitter process, additive signal averaging will eventually converge to a smooth estimate of the measured waveform, as with the y-axis noise case, but unlike the y-axis noise averaging, the resulting waveform estimate will be quite distorted. Fig. 4 is a modeled illustration of the effects of additive signal averaging in the presence of time jitter only. The true measured waveform in this illustration is a triangular pulse but the sig-

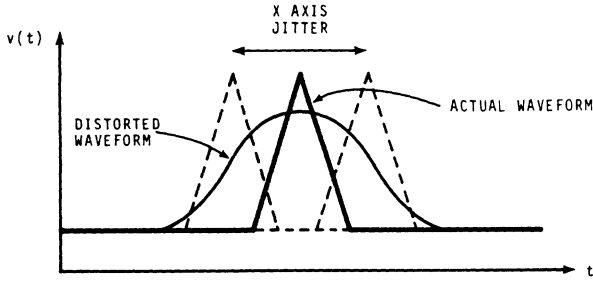


Fig. 4. Modeled illustration of the effects of time jitter alone. Triangular pulse, sampled and additively averaged, would result in a smoothed, distorted recorded waveform.

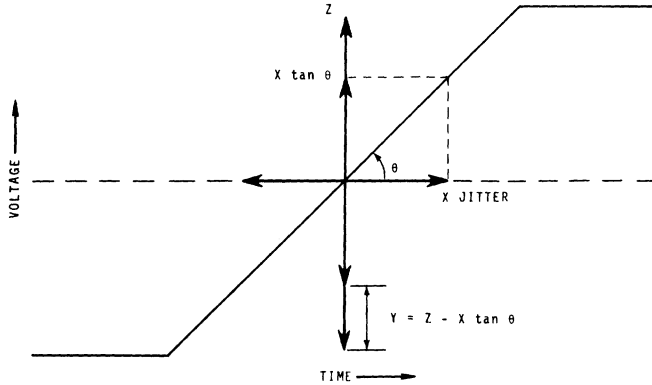


Fig. 5. Graphical illustration of the model and technique for finding $p(x)$ and $p(y)$ from $p(z)$ and θ on a modeled ramp function.

nal-averaged recorded waveform will look something like the smooth, distorted waveform superimposed. The problem, then, is to somehow recover the true waveform from the distorted, measured waveform data.

Fig. 5 is a graphical representation of how this may be done. For the modeled ramp waveform shown, with the ramp portion of the waveform lying at an angle θ to the abscissa, voltage samples are acquired nominally as near as possible to the vertical center of the ramp. These samples, in the presence of both y -axis noise and x -axis jitter, will be randomly distributed and will be a function of both noise processes. In particular, each acquired sample can be written

$$v_m(t) = v_a(t) + v_x(t) + v_y(t) \quad (8)$$

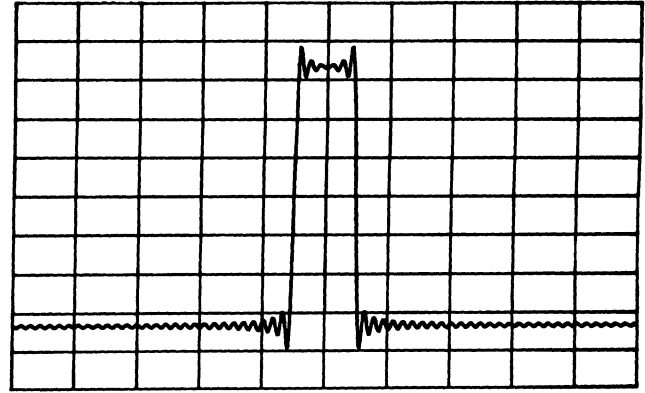
where $v_m(t)$ is the measured voltage sample value, $v_a(t)$ is the actual (true) value of the ramp at that time point, $v_y(t)$ is the added vertical noise component for that sample, and $v_x(t)$ is the difference in the ramp voltage due to the fact that the time jitter really caused the sample to be taken at a different point in time than the presupposed one.

These sample observations may be thought of as observations of a random variable Z which, in turn, is the sum of two random variables Y and a function of X . Since the voltage samples perturbed only by the x -axis jitter will always lie on the true waveform (the ramp in this illustration) then the observed random samples will be of the random variable $X \tan \theta$. Z then can be expressed as

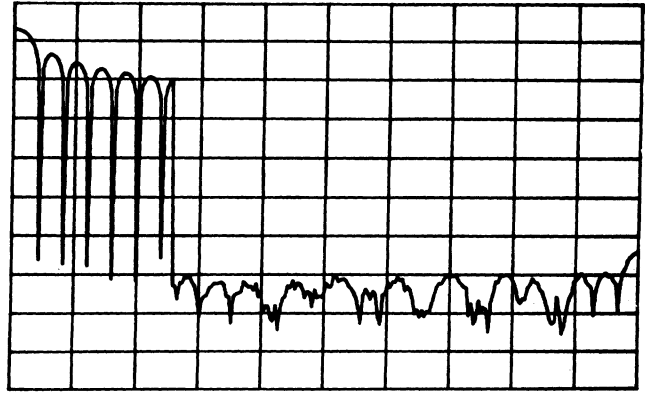
$$Z = Y + X \tan \theta \quad (9)$$

where Z , Y , and X are all random variables [1], [2].

The objective at this point is to find the Probability Density



(a)



(b)

Fig. 6. (a) Test waveform consisting of the summation of first 64 Fourier harmonics of a 2-V, 0.1-s rectangular pulse. Vertical scale is 300 mV/division and horizontal scale is 0.1 s/division. (b) Spectrum magnitude of (a). Vertical scale is 28 dB/division (top line = 0 dB) and horizontal scale is 25.6 Hz/division.

Function (PDF) for X , $p_X(x)$, and, treating it as an effective, jitter-related impulse response, deconvolve it from the recorded, signal-averaged waveform.

For the sum of two independent random variables, it may be shown [7] that

$$p_Z(z) = p_Y(y) * p(x \tan \theta)$$

where the $*$ denotes the convolution operation. Also it may be shown [8] that variables may be changed such that

$$p(x \tan \theta) = \frac{1}{\frac{d(x \tan \theta)}{dx}} p_X(x)$$

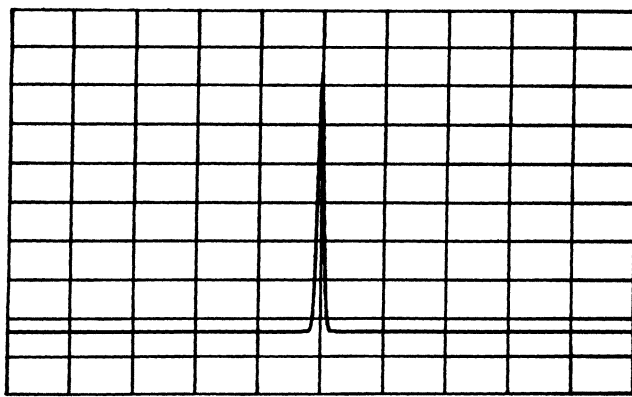
or

$$p_X(x) = p(x \tan \theta) \tan \theta. \quad (10)$$

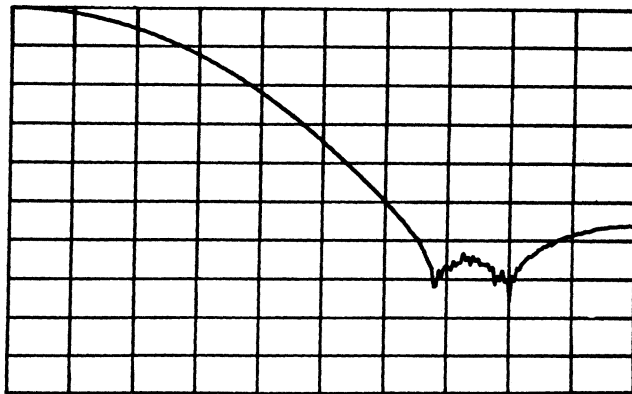
Therefore, by measuring $p_Z(z)$, θ , and $p_Y(y)$ (the latter being measured with either no applied signal or on a zero-slope portion of the measured signal), $p(x)$ may be estimated. The steps for the estimation of $p_X(x)$ are as follows:

- measure the histogram for $p_Z(z)$
- measure the histogram for $p_Y(y)$
- deconvolve $p_Y(y)$ from $p_Z(z)$ to yield $p(x \tan \theta)$
- calculate $p_X(x)$ from $p(x \tan \theta)$ using (10).

In the case where the slope of the true function is not constant



(a)



(b)

Fig. 7. (a) Gaussian probability density function/impulse response. Vertical scale is $1.2 \times 10^4 \text{ s}^{-1}$ /division and horizontal scale is 0.1 s/division. Standard deviation (σ) is 0.005 s. (b) Spectrum magnitude of (a). Vertical scale is 20 dB/division (top line = 0 dB) and horizontal scale is 25.6 Hz/division.

in the neighborhood of the measurement of $p_Z(z)$, a linear least squares curve fit through the nominal time sampling point may be used to correct the $p_Z(z)$ data.

Once $p_X(x)$ has been estimated, it then can be deconvolved from the previously recorded, signal-averaged waveform to yield an estimate of the true waveshape with the disturbing effects of the time jitter effectively removed.

III. COMPUTER SIMULATIONS

In order to establish the efficacy of this deconvolution approach to removing the distorting effects of time jitter from measured waveform data, a set of computer simulation experiments was performed. The approach used was to generate 512-point test waveforms in the computer, create jittery versions of the test waveform using a random number generator with a known PDF, additively average the jittery test waveforms, deconvolve the jittery averaged waveform from the 512-point PDF function, and then compare the result with the original test function.

Fig. 6(a) is a plot of one of the test waveforms used, in this case the sum of the first 64 Fourier harmonics of a 2-V, 0.1-s rectangular pulse in a 1-s time window. Fig. 6(b) is a plot of the discrete Fourier spectrum magnitude of this test function. Test functions, band-limited such as this, were chosen to minimize the adverse effects of aliasing when performing the fast Fourier transforms in the deconvolution algorithm.

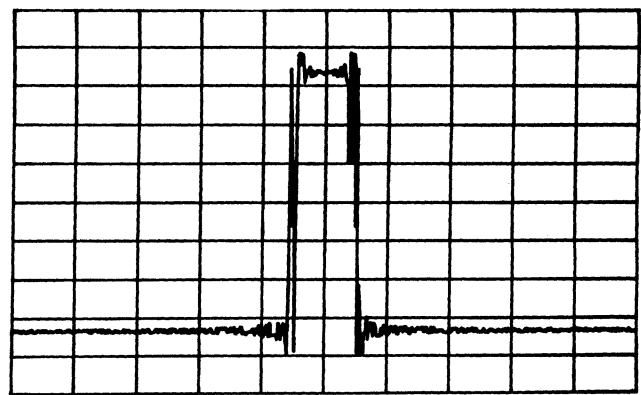
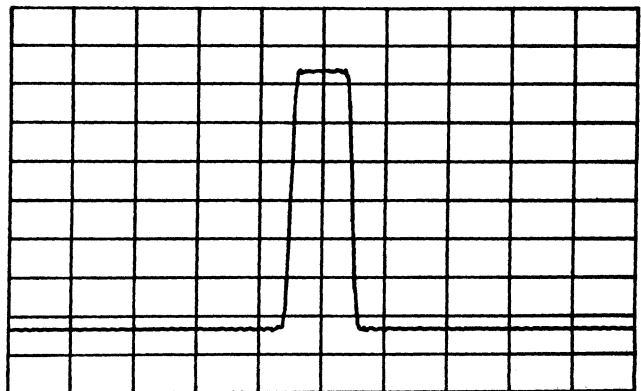
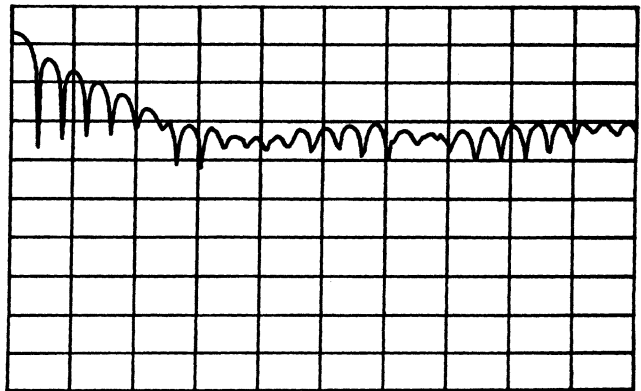


Fig. 8. Typical test waveform with applied time jitter. Vertical scale is 300 mV/division and horizontal scale is 0.1 s/division.



(a)



(b)

Fig. 9. (a) 100 additive averages of time-jittered test waveforms. Vertical scale is 300 mV/division and horizontal scale is 0.1 s/division. (b) Spectrum magnitude of (a) with vertical scale of 20 dB/division (top line = 0 dB) and horizontal scale of 25.6 Hz/division.

Fig. 7 is a plot of the x-axis jitter PDF used in this particular experiment. This PDF is a Gaussian (normal) PDF with a standard deviation σ of 0.005 s. Its amplitude has been normalized to fit the requirements of being both a PDF and an impulse response, i.e., its integral over the time window equals 1. Fig. 7(b) is a plot of the discrete Fourier spectrum magnitude of this PDF.

Next, the test function of Fig. 6(a) was corrupted with time jitter. The random numbers causing this jitter were generated from a nonrepeating Gaussian random number generator with σ also set to 0.005 s. The jittered waveforms were produced by changing the index of each test function sample point ran-

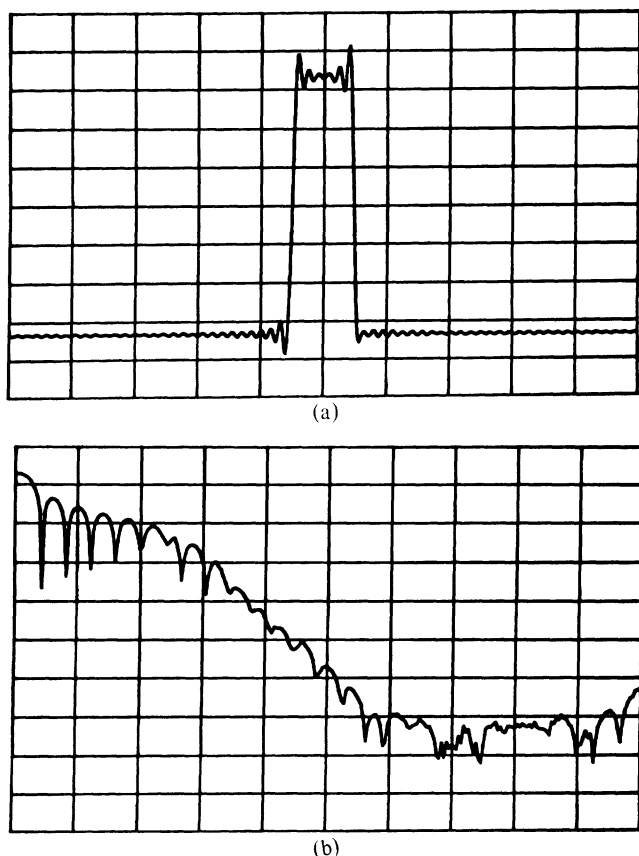


Fig. 10. (a) Deconvolution of waveforms shown in Figs. 7(a) and 9(a). Vertical scale is 300 mV/division and horizontal scale is 0.1 s/division. (b) Spectrum magnitude of (a). Vertical scale is 20 dB/division (top line = 0 dB) and horizontal scale is 25.6 Hz/division.

domly. For example, in a given run, the value of $V(148)$ might be substituted by the value of $V(157)$. Fig. 8 is a plot of one such jittered version of the test waveform.

The next step was to add up and average N such jittery waveforms to simulate the additive averaging performed on the APMS. Trials of $N = 100$, 1000, and 10 000 were attempted in order to observe the effects of varying the number of averages.

Fig. 9(a) is a plot of 100 averages of the jittered test function. This plot is fairly smooth but appears to be quite different from the original test function of Fig. 6(a). Fig. 9(b) is a plot of the spectrum magnitude of this averaged jittered test waveform and again, appears quite different from the original test waveform spectrum of Fig. 6(b).

Fig. 10(a) is a plot of the deconvolution of the Gaussian effective impulse response of Fig. 7(a) and the averaged, jittered test waveform of Fig. 9(a). Fig. 10(b) is a plot of the spectrum magnitude of this deconvolved result. If the jitter deconvolution had worked perfectly then the two waveforms of Figs. 6(a) and 10(a) would be identical. Fig. 11 is a plot of the point-by-point error difference between the two waveforms expressed as a percentage of the 2-V nominal original pulse amplitude. As shown, the peak error exceeds 10 percent.

Repeating the same experiment but with N equal to 1000 averages, the averaged jittered waveform of Fig. 12 results. Deconvolving this waveform and the Gaussian PDF yields the estimated true waveform shown in Fig. 13. The error difference

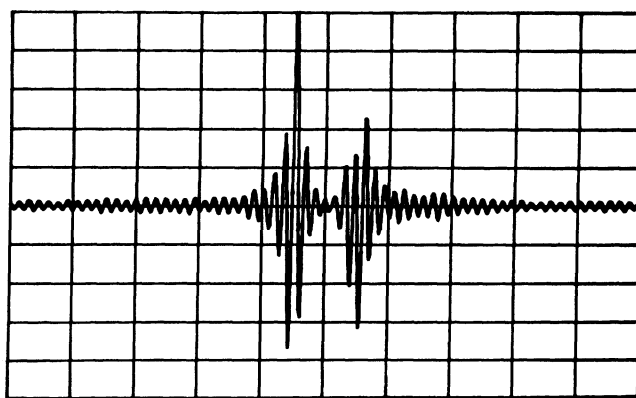


Fig. 11. Point-by-point error difference between waveforms shown in Figs. 6(a) and 10(a). Vertical scale is 2 percent (of 2 V)/division and horizontal scale is 0.1 s/division.

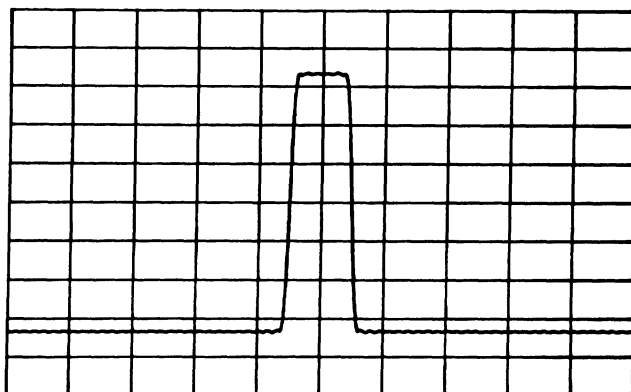


Fig. 12. 1000 additive averages of time-jittered test waveforms. Vertical scale is 300 mV/division and horizontal scale is 0.1 s/division.

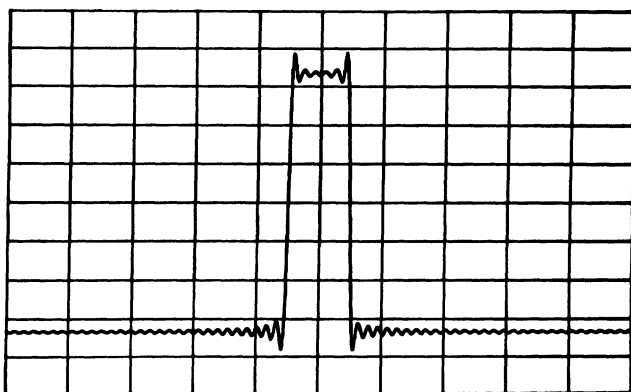


Fig. 13. Deconvolution of waveforms shown in Figs. 7(a) and 12. Vertical scale is 300 mV/division and horizontal scale is 0.1 s/division.

between the original test waveform and the deconvolved estimate is shown in Fig. 14. For 1000 averages, the peak error has dropped to approximately 4 percent.

By setting N equal to 10 000 averages the averaged, distorted waveform of Fig. 15(a) results. Its spectrum magnitude is shown in Fig. 15(b). After jitter deconvolution, the true waveform estimate of Fig. 16(a) results and its spectrum magnitude is shown in Fig. 16(b). The comparison of Figs. 6(a) and 16(a) (or Figs. 6(b) and 16(b)) indicate a close agreement between the two. Fig. 17, a plot of the error difference of these two waveforms, bears out this agreement, exhibiting a peak error difference of only 2 percent.

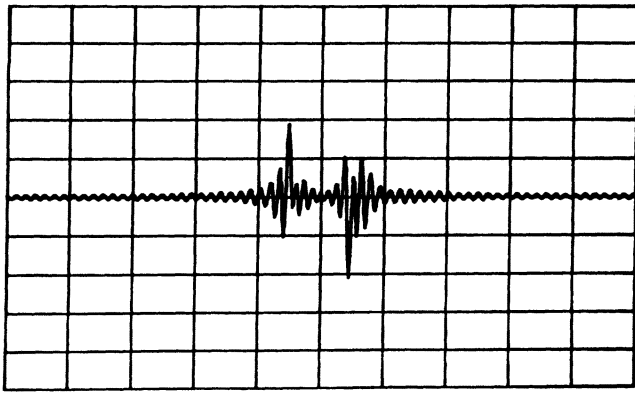
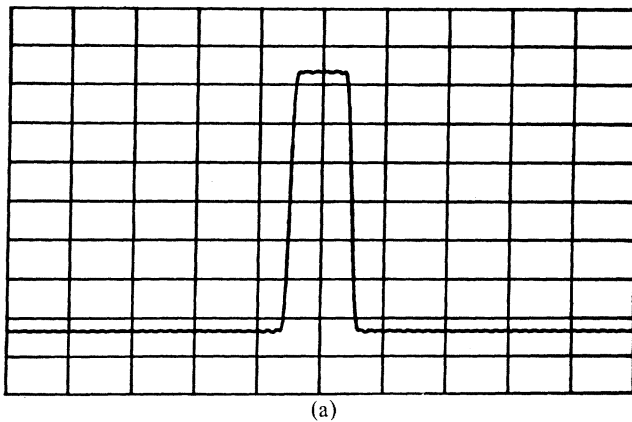
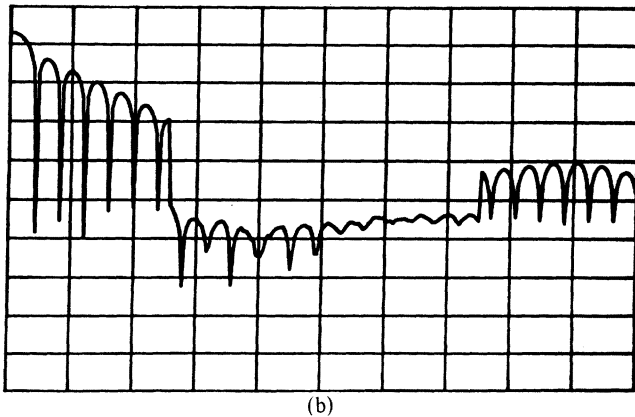


Fig. 14. Point-by-point error difference between waveforms shown in Figs. 6(a) and 13. Vertical scale is 2 percent (of 2 V)/division and horizontal scale is 0.1 s/division.



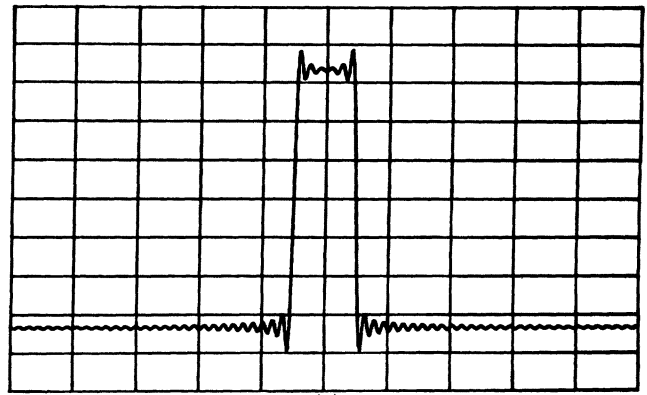
(a)



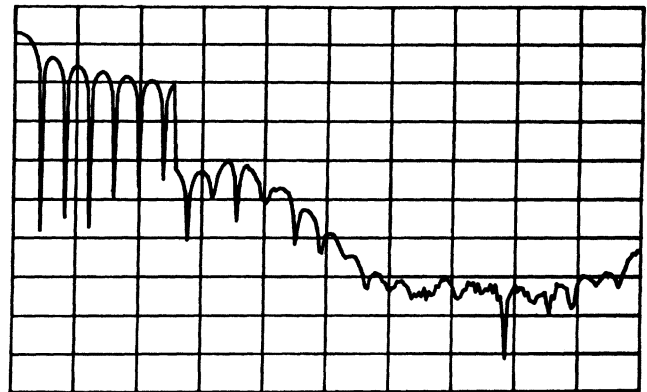
(b)

Fig. 15. (a) 10 000 additive averages of time-jittered test waveforms. Vertical scale is 300 mV/division and horizontal scale is 0.1 s/division. (b) Spectrum magnitude of (a). Vertical scale of 20 dB/division (top line = 0 dB) and horizontal scale of 25.6 Hz/division.

To set a bound on how well this technique could be expected to work, another experiment was performed. The test waveform of Fig. 6(a) was convolved directly in the time domain, using (1), with the Gaussian jitter function of Fig. 7(a). This result was then deconvolved from the jitter function of Fig. 7(a) using the Nahman-Guillaume algorithm. When the resulting test function was compared to the original test function of Fig. 6(a), the point-by-point error difference of Fig. 18 resulted. Except for some small errors at the time window extremes due to leakage errors in the fast Fourier transform, this experiment appears to indicate that much smaller errors than those observed in Fig. 17 are achievable.



(a)



(b)

Fig. 16. (a) Deconvolution of waveforms shown in Figs. 7(a) and 15(a). Vertical scale is 300 mV/division and horizontal scale is 0.1 s/division. (b) Spectrum magnitude of (a). Vertical scale is 20 dB/division (top line = 0 dB) and horizontal scale is 25.6 Hz/division.

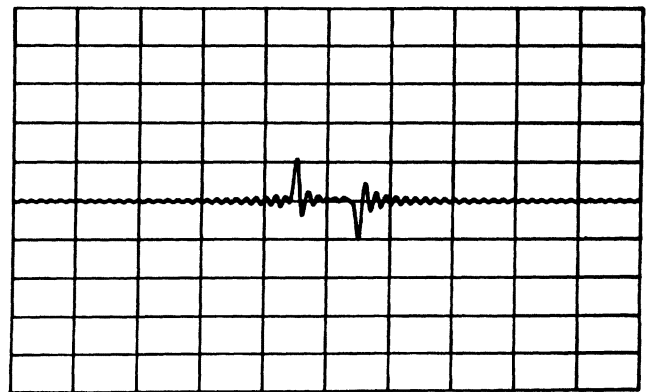


Fig. 17. Point-by-point error difference between waveforms shown in Figs. 6(a) and 15(a). Vertical scale is 2 percent (of 2 V)/division and horizontal scale is 0.1 s/division.

After completing many sets of computer simulation experiments such as the one described above, it became apparent that the success or failure of the jitter-deconvolution technique is a function of several variables. The test waveform bandwidth, the effective jitter-related impulse response bandwidth, the number of jittery signal additive averages, and the number precision of the computer (in this case approximately 6 decimal digits) all play a role in determining how well the original test signal may be recovered. As an approximate rule of thumb, it was observed that good results were obtained, with large numbers of additive averages, as long as the spectrum of the jitter-related impulse response was no greater than 30 dB

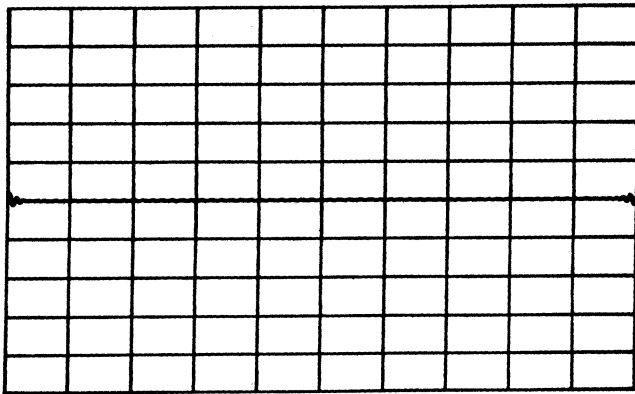


Fig. 18. Point-by-point difference between test waveform of Fig. 6(a) and the same waveform convolved and then deconvolved from Gaussian jitter function of Fig. 7(a). Vertical scale is 2 percent (of 2 V)/division and horizontal scale is 0.1 s/division.

below its fundamental spectrum magnitude at the frequency at which the test waveform's spectral energy becomes negligibly small. Also, it was noted that unstable results were occasionally observed when the number of additive signal averages was less than 500.

IV. CONCLUSIONS

A method has been described for removal of the distorting effects of time jitter present in equivalent-time waveform samplers. This method involves determining the PDF of the time axis jitter, treating that PDF as a time-domain impulse response, and deconvolving it from the recorded, additively averaged waveform of interest. As long as the jitter is not excessive and as long as a sufficient number of additive signal

averages are acquired, peak errors of less than ± 2 percent may be realized. The techniques described in this paper may also be used for only the *measurement* of jitter-related noise parameters, such as the rms jitter within fast logic gates, for example.

Efforts are continuing at NBS to refine the method and to identify more exactly the sources of error and the various parameter regions of convergence. Additional work also remains in the area of obtaining measured PDF's on the APMS under various sampling oscilloscope triggering conditions.

REFERENCES

- [1] W. L. Gans, "A time domain automatic network analyzer for microwave measurements," M.S. Thesis, Univ. of Colorado, Boulder, CO, Spring 1975.
- [2] W. L. Gans and J. R. Andrews, "Time domain automatic network analyzer for measurement of RF and microwave components," NBS Tech. Note 672, Sept. 1975.
- [3] W. L. Gans, "Present capabilities of the NBS automatic pulse measurement system," *IEEE Trans. Instrum. Meas.*, vol. IM-25, pp. 384-388, Dec. 1976.
- [4] S. M. Riad, "The theory and application of the homomorphic transformation to time domain spectroscopy and scattering problems," Ph.D. dissertation, Univ. of Toledo, Toledo, OH, Aug. 1976.
- [5] S. M. Riad and N. S. Nahman, "Modeling of the feed-through wideband (dc to 12.4 GHz) sampling head," in *Dig. 1978 IEEE-MTT-S Int. Microwave Symp.* (Ottawa, Ont., Canada, June 27-29, 1978).
- [6] N. S. Nahman and M. E. Guillaume, "Deconvolution of time domain waveforms in the presence of noise," NBS Tech. Note 1047, Oct. 1981.
- [7] M. E. Guillaume and J.-C. Bizeul, "Impulse response of a transmission medium: Application to optical fibers" (in French), *Annales des Telecommunications*, vol. 36, nos. 3-4, pp. 179-185, Mar.-Apr. 1981.
- [8] P. Beckman, *Probability in Communication Engineering*. New York: Harcourt, Brace and World, 1967, pp. 75-76.
- [9] J. S. Bendat, *Principles and Applications of Random Noise Theory*. New York: Wiley, pp. 1958, 114-115.